frontiers in Materials

ORIGINAL RESEARCH
published: 13 May 2021
doi: 10.3389/fmats.2021.668835

Self-Supported Smart Bacterial Nanocellulose–Phosphotungstic Acid Nanocomposites for Photochromic Applications

Moliria V. Santos[1], Hernane S. Barud[2], Monica A. S. Alencar[1], Marcelo Nalin[1], Sérgio H. Toma[3], Koiti Araki[3], Assis V. Benedetti[1], Indhira O. Maciel[4], Benjamin Fragneaud[4], Cristiano Legnani[1,4], Celso Molina[5], Marco Cremona[6] and Sidney J. L. Ribeiro[1]**

[1] Institute of Chemistry – São Paulo State University (UNESP), Araraquara, Brazil, [2] Laboratório de Biopolímeros e Biomateriais (BioPolMat), Universidade de Araraquara, Araraquara, Brazil, [3] Instituto de Química – Universidade de São Paulo (USP), São Paulo, Brazil, [4] Departamento de Física, Instituto de Ciências Exatas, Universidade Federal de Juiz de Fora (UFJF), Juiz de Fora, Brazil, [5] Deparment of Chemistry, Federal University of São Paulo, (UNIFESP), Diadema, Brazil, [6] Departamento de Física, Pontifícia Universidade Católica do Rio de Janeiro (PUC-Rio), Rio de Janeiro, Brazil

OPEN ACCESS

Edited by:
Wenbo Wang,
Inner Mongolia University, China

Reviewed by:
Jin Yang,
Shaanxi University of Science and Technology, China
Walter Caseri,
ETH Zürich, Switzerland

***Correspondence:**
Hernane S. Barud
hernane.barud@gmail.com
Sidney J. L. Ribeiro
sidney.jl.ribeiro@unesp.br

Specialty section:
This article was submitted to Polymeric and Composite Materials, a section of the journal Frontiers in Materials

Received: *26 February 2021*
Accepted: *19 April 2021*
Published: *13 May 2021*

Citation:
Santos MV, Barud HS, Alencar MAS, Nalin M, Toma SH, Araki K, Benedetti AV, Maciel IO, Fragneaud B, Legnani C, Molina C, Cremona M and Ribeiro SJL (2021) Self-Supported Smart Bacterial Nanocellulose–Phosphotungstic Acid Nanocomposites for Photochromic Applications. Front. Mater. 8:668835. doi: 10.3389/fmats.2021.668835

Bacterial nanocellulose (BNC) is a natural biopolymer obtained by gram-negative bacteria by means of a green and inexhaustible biotechnological process using glucose as producing source. BCN hydrogels is formed by cellulose nanofibrils that maintain an open network structure, an ideal matrix to produce new class of organic-inorganic nanocomposites (OIN) for multifunctional applications. The polyoxometalates (POMs) are complex molecules with several metallic ions sharing oxide ions, forming a highly symmetrical metal oxide cluster. Phosphotungstic acid (PWA), $H_3PW_{12}O_{40}$ photoreduction process activated under ultraviolet irradiation, promoting color change. In this work, photochromic organic-inorganic nanocomposites were prepared by soaking phosphotungstic acid ($H_3PW_{12}O_{40}$) in wet BNC membranes mats at room temperature. Semi-transparent and free-standing BNC/PWA nanocomposite with paper-like aspect were obtained. BNC network was able to control, stabilize and disperse PWA particles in a narrow nanometric distribution, and FTIR spectra indicated that the primary Keggin structure was also preserved in the nanocomposites, independently on the PWA content. The nanoparticles present a narrow distribution of around 16 nm, independently on the PWA concentration. BNC/PWA nanocomposites showed reversible photochromic behavior characteristic of the equilibrium between different tungsten oxidation states. PWA reduction ($W^{6+} \rightarrow W^{5+}$) and organic matrix oxidation is proposed to occur through a radical process involving the interaction of one electron from the oxygen atom of the PWA and one hydrogen from BNC matrix. The photochromic effect vanishes almost completely after 5 h. This mechanism is real in the

presence of oxygen, however, if the membranes are left in nitrogen or under vacuum the blue color remains longer than 45 days. Photo-electrochemical behavior was studied by spectroelectrochemistry measurements. It is worth noting that all processes were still reversible in the timescale of the experiment and color changes were observed in several cycles.

Keywords: bacterial nanocellulose, photochromism, polyoxometalates, phosphotungstic acid, electrochromism

INTRODUCTION

Bacterial nanocellulose (BNC) is a versatile and unique biopolymer nanomaterial produced by gram-negative bacteria such as *Komagateibacter genus* using a green and inexhaustible biotechnological process (Ross et al., 1991; Klemm et al., 2005). Differently of plant cellulose process extraction, BNC is produced by green and inexhaustible biotechnological route and its obtaining free of impurities in 3-D hydrogel network structure formed by nanocellulose. When produced in a static culture medium, BNC hydrogel displays transparency, moldability and higher mechanical strength and crystallinity than cellulose from plants (Azeredo et al., 2019). The obtained BNC hydrogel is free of impurities (lignin, hemicelluloses and pectin) and it is formed by a three-dimensional nanostructure of bundles of cellulose nanofibrils. BNC hydrogel displays transparency, moldability and higher mechanical strength and crystallinity than cellulose from plants (Eichhorn, 2001; Klemm et al., 2001; Svensson et al., 2005). These properties combined with the fact that BNC presents an open network structure, allow the incorporation of organic/inorganic compounds in its structure leading to new organic-inorganic nanocomposites (OIN) for multifunctional applications (medical, food, pharmacy and optoelectronics) (Eichhorn et al., 2010; Gatenholm and Klemm, 2010; Klemm et al., 2011; Azeredo et al., 2019; Bretel et al., 2019; Legnani et al., 2019; Torres et al., 2019; Chiozzini et al., 2020; Dong et al., 2020; Yang et al., 2021).

The photochromic behavior of bacterial nanocellulose/spiropyran nanofibrous membranes has been reported previously (Hu et al., 2011). BNC/spiropyran photochromic membranes showed reversible photochromic behavior since change color from colorless to pink forming a merocyanine structure upon UV irradiation, and turn back to colorless spiropyran structure by irradiation with visible light.

In the same way, Gutierrez et al. demonstrated that BNC can be used as templates for fabrication of conductive and photochromic vanadium nanopapers via sol-gel process (Gutierrez et al., 2012). The trend in photochromism gained momentum upon synergistic combination with other materials in order to generate new functional materials. Growing interest in this field led to the improvement of existing photochromic materials, fabrication of photoresponsive devices while exploring new families of photochromic materials, such as organic-inorganic photochromic hybrid systems based on transition metal oxides and polyoxometalates (Chen et al., 2000; He et al., 2001; He and Yao, 2006; Qi and Wu, 2009; Dufaud and Lefebvre, 2010).

Polyoxometalates (POMs) are complex molecules with several metallic ions coordinated by shared oxide ions, forming highly symmetrical metal clusters. They are good candidates as functional molecules to be incorporated in organic-inorganic matrices due to their structures and properties. The metallic ions in the POM structure are susceptible to reversible redox process and becoming colored species due to the formation of mixed valence cations (heteropolyblues and heteropolybrowns). Its redox property and high-density of electrons are ideal for use in photo and electrochromic materials (Yamase, 1998). However, it is difficult to prepare films using only POM compounds what limits their applications. Nowadays, POM nanoparticles are been entrapped into polymeric networks to get transparent thin films and to improve their photochromic properties and stability (Casan-Pastor and Gomez-Romero, 2005; He and Yao, 2006; Chen et al., 2008; Qi and Wu, 2009). Organic polymers are easily processed and shaped, in addition to present excellent toughness and ductility, making them suitable for applications as matrices for incorporation of POMs (Feng et al., 2002; Espindola et al., 2019).

Taking into account the good solubility in water-based and polar solvents, phosphotungstic acid (PWA), represented by $H_3PW_{12}O_{40}$ molecular formula, is one of the most important POM that has been explored in the preparation of new OINs. Besides that, PWA has defined size Keggin's structure where the change of color is mainly due to the photoreduction of its W^{6+} sites under ultraviolet irradiation (Cruz et al., 2017).

Cruz et al. have obtained a photochromic hybrid material based on the incorporation of di-ureasil and PWA on flexible recycled PET (Cruz et al., 2017). Moreover, Espíndola et al., have obtained highly transparent polymethylmethacrylate – PWA with fast photochromic response by using drop-on-demand inkjet (DOD) technology for miniatured devices (Espindola et al., 2019).

Herein, we report for the first time the preparation and full characterization of photochromic self-sustainable flexible nanocomposites based on BNC membranes and PWA, and their photochromic and electrochromic compared. Here, we would like to highlight that, to the best of our knowledge, there is no report yet comparing these processes.

The evaluation of structural and morphological results by FTIR and TEM confirms that PWA Keggin structure was preserved inside the BNC/PWA nanocomposites in narrow nanometric size scale distribution. Photo-electrochromic effect by spectroelectrochemical and RAMAN spectroscopy were successfully performed to elucidate photochromic behavior of different tungsten oxidation states.

MATERIALS AND METHODS

Bacterial Cellulose Preparation

The strain used for BNC production was *Gluconacetobacter xylinus* (ATCC 23760) supplied by André Tosello Foundation, Campinas-SP, Brazil. It was cultured in Hestrim-Schramm medium (HS medium) containing D-glucose glycose, yeast extract, peptone, di-sodium hydrogen phosphate (Na_2HPO_4), citric acid, agar and purified water. Analytical grade chemicals were used as received. Before the bacterial strain inoculation, the strain culture medium was sterilized and then cultivated for 1 day at 28°C in an air circulating oven as conditioning chamber. The BNC culture medium was prepared according to the previously reported method. 45 mL of culture medium and 5 mL of the inoculum were cultivated for 3 days in static conditions at 28°C in a 250 mL Erlenmeyer flask in an air circulating oven. After this time, BNC hydrogel was harvested and purified to eliminate the culture medium (to remove the cells and other impurities). The purification protocol was realized following a previously described protocol (Tercjak et al., 2015).

BNC Nanocomposites Preparation

Wet 3 mm thick BNC membranes (6 cm × 6 cm) were immersed in a 250 mL Erlenmeyer flask containing 25 mL of PWA (Sigma-Aldrich) solution with different concentrations related to BNC area (cm^2). PWA 15% w/area, 30% w/area and 50% w/area. Afterward the samples were set in motion using a stirring table for 96 h, at room temperature. BNC/PWA nanocomposites were washed five times using 20 mL of distilled water (each time) at room temperature. This procedure was applied to remove the excess of the PWA from the surface of BNC. The average thickness of BNC/PWA was ∼40 μm and the concentration of PWA in the nanocomposites was estimated from the residues obtained in thermogravimetric (TGA) tests performed in an oxidizing environment at 600 °C. The resulting PWA contents were 13.5% w/w, 35.5% w/w and 49.5% w/w. BNC/PWA nanocomposites were renamed accordantly PWA contents: BNC/PWA 13.5%, BNC/PWA 35.5% and BNC/PWA 49.5%.

Methods

The morphology of the nanocomposites was investigated using a JEOL 200CX transmission electron microscope (TEM). To prepare the samples, the nanocomposites membranes were powdered in the presence of liquid nitrogen and suspended in absolute ethanol Sigma (0.01% weight/volume). A drop of the as-prepared suspension was placed onto the surface of Lacey formvar/carb 300-mesh copper grid and followed by evaporation of the solvent. The photochemical behavior was studied by UV-vis using a Varian Cary 500 spectrophotometer with 1 nm optical resolution, in the 100–2,000 nm range. Photochromic experiments were carried out using a box containing 3 lamps with 27 mW power and emission wavelengths between 300 and 370 nm. The distance between the lamps and samples was 10 cm and the exposure time was 15 min. The material was structurally characterized by infrared spectroscopy (FTIR) using a Perkin-Elmer spectrometer, model 2000 in the range from 400 to 4,000 cm^{-1}. The hybrids were milled and mixed with dried KBr in 1:100 proportions and pressed into pellets. Raman spectra were recorded using a Raman HORIBA JOBIN–YVON model LabRAM HR 800 spectrometer, operating with He–Ne laser at 632.8 nm equipped with a CCD camera model DU420AOE-325. Electrochemical measurements were carried out with a Microquímica MQPG instrument and a coupled Quimis stereoscopic microscope. Cyclic voltammograms were obtained using two platinum wires as auxiliary electrode, $Ag/AgCl/KCl_{sat}$ as reference electrode and the working electrode was a modified carbon paste electrode (CPE) with the prepared composites and 0.2 M Na_2SO_4 solution, adjusted to pH 2 with 5 mM H_2SO_4, as electrolyte. To increase the physical contact between electrode and BNC/PWA nanocomposites, the membranes were previously milled. Spectroelectrochemical measurements were carried out with an EG&G PAR 173 potentiostat/galvanostat coupled with a Guided Wave fiber optic spectrophotometer model 260, operating in transmittance mode between 400 and 1,700 nm. OINs BNC/PWA nanocomposites membranes were assembled in a three-electrode system device composed by two fluorine doped tin oxide coated glass (FTO) electrodes and $Ag/AgCl/KCl_{sat}$ luggin capillary as reference electrode. To avoid short circuit between FTO electrodes, a 150 μm thick frame layer of thermo-sealing film Surlyn® was applied at opposite edges of OINs BNC/PWA membrane, pressing it on the working electrode and then sandwiched with the FTO glass counter electrode. The thermo-sealing was melted with a hot air gun and immediately clamped to ensure a tight sealing. The device was partially immersed in 0.2 M Na_2SO_4, pH 2 by one of the free ends, filling the electrodes gap and then the reference electrode was positioned facing the bare edge of the working electrode in the immersed portion of the device. Cyclic voltammograms were obtained from +1.0 to −0.75 V/($Ag/AgCl/KCl_{sat}$) at different scan rates and spectroelectrochemical data collected at stationary mode, with 5 to 10 mV steps between each spectrum.

RESULTS

Morphological Characterization

The incorporation of PWA occurred by simple diffusion through the pores of hydrated BNC membranes, and the final thickness of all BNC-based nanocomposites were maintained in ∼40 μm.

After drying processes, BNC/PWA OINs exhibited paper-like aspect, macroscopically homogeneous, free-standing, semi-transparent and flexible, as shown in **Figures 1A–C**. The blue color of **Figures 1B,C** arises from the BNC/PWA membranes exposition to ultraviolet radiation. It is noteworthy that even after irradiation membranes remain semi-transparent.

Transmission electron microscopy images were obtained for the OIN and the results are shown in **Figure 2**. The nanoparticles are uniformly distributed and have spherical shape. This allows to consider that the tri-dimensional BNC nanofibers act controlling, stabilizing and dispersing the PWA particles as shown in **Figure 2A** (Barud et al., 2008; Gutierrez et al., 2012). The PWA

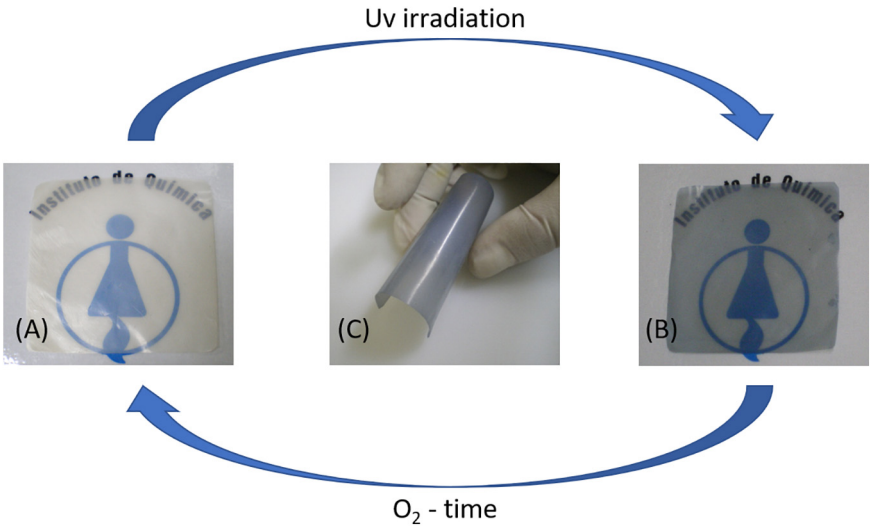

FIGURE 1 | Pictures of BNC/PWA 49.5% before **(A)** and after irradiation **(B)**. The photochromic effect vanishes almost completely after 5 h under ambient conditions. In panel **(C)** the flexible behavior is showed.

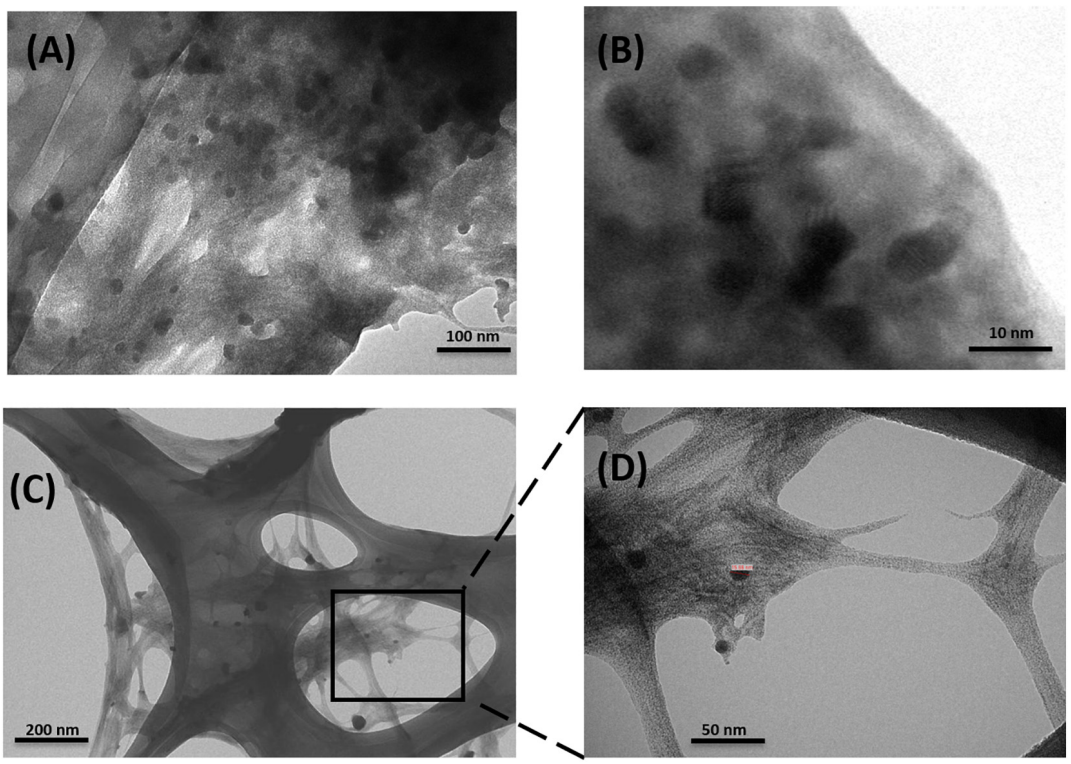

FIGURE 2 | Transmission electron micrograph image of **(A,B)** BNC/PWA 49.5% and **(C,D)** BNC/PWA 13.5%.

spherical nanoparticles present a narrow distribution of around 16 nm, independently the PWA concentration.

Structural Characterization

The IR spectra of PWA (**Figure 3**) present four characteristic bands at 1,081, 982, 888, and 801 cm^{-1} assigned to stretching vibration $\nu(P–O_a)$, $\nu(W–O_d)$, $\nu(W–O_b–W)$ and $\nu(W–O_c–W)$(Bridgeman, 2003), respectively, characteristic of the Keggin units (Rocchiccioli-Deltcheff et al., 1976).

FTIR spectra indicated that the primary Keggin structure was preserved inside the nanocomposites. It also showed a widening of the W-O_d, W-O_b-W, and W-O_c-W vibrational modes and

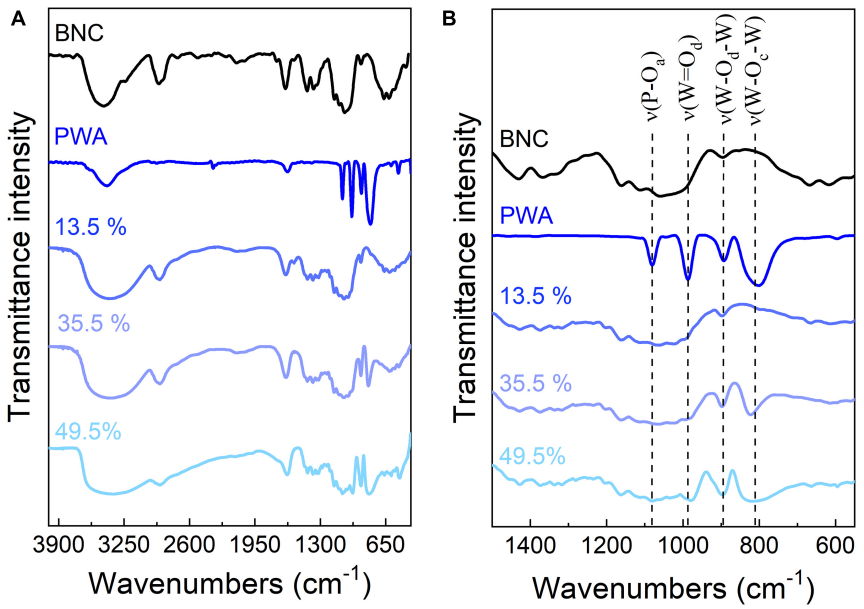

FIGURE 3 | (A) FTIR spectra of BNC, PWA, BNC/PWA 13.5, 35.5, and 49.5%. **(B)** Zoom of the spectra shown in panel **(A)** for better visualization of the changes in the bands between 600 and 1,200 cm^{-1}.

the shift of some vibration bands, like those assigned to the W-O_d and W-O_c-W modes (**Table 1**). These changes should be attributed to strong interactions of electrostatic nature between PWA and the polymer matrix, due to the heteropolar character of PWA (Katsoulis, 1998).

Raman spectra were also obtained for the irradiated BNC/PWA 49.5% sample during the reversible process. **Figure 4** shows the Raman spectra of the samples. **Figure 5** is a detailed view of the Raman spectrum in the range of 960 cm^{-1} to 1,040 cm^{-1}. This region is related to the polyoxometalate main Raman features. The spectrum on **Figure 5** has been fitted with four bands with a Lorentzian spectral line shape centered at 1,012 cm^{-1}, 1,008 cm^{-1}, 990 cm^{-1} and 977 cm^{-1}. A. J. Bridgeman has thoroughly analyzed the symmetry of Raman active mode of the a-Keggin polyanion, and obtained the expected values of such vibration modes with DFT calculations (Bridgeman, 2003). It comes out that the peak at 1,012 cm^{-1} corresponds to the symmetric stretching of the W-O_t bonds, ν_s(W–O_t). O_t stands for the most outward oxygen atoms of the octahedra surrounding the tungsten atom. The other three peaks are asymmetric vibrations modes of the (W–O_t) corresponding the irreducible representations e, t_1 and t_2, respectively. The spectrum on **Figure 5A**, which corresponds to the unexposed samples, exhibits essentially the contribution of the peak corresponding to the symmetric vibrations of the W–O_t bounds. However, **Figure 5B**, that corresponds to the Raman spectrum of irradiated samples, presents some notable changes. For instance, the intensity ratio of the peaks at 1,012 cm^{-1} and 1,008 cm^{-1} went from 1.44 for unexposed samples to 0.17 for irradiated ones, meaning that the symmetric band contribution almost disappeared. This is an evidence that the irradiation process changes the octahedral arrangement around the W atoms when a number of species is reduced from W^{6+} to W^{5+}. Indeed, it seems that the most outward atoms, which are more sensible to the oxidation process, are undergoing some chemical reaction thus breaking the symmetry of the W–O_t bounds arrangement. Also, the main asymmetric W–O_t peak at 1,008 cm^{-1} substantially shifts to lower energies, most probably due to the transition of tungsten oxidation number situated at the center of the octahedra. Finally, on **Figure 5C**, it is striking how the spectrum goes back to its original form when removing UV exposure. This indicates that the process is perfectly reversible.

TABLE 1 | Characteristic bands of the PWA Keggin structure.

Samples	ν(P–O_a) (cm^{-1})	ν(W-O_d) (cm^{-1})	ν(W–O_b–W) (cm^{-1})	ν(W–O_c–W) (cm^{-1})
PWA	1081	988	892	801
BNC/PWA 13,5%	–	–	898	–
BNC/PWA 39.5%	–	–	896	822
NC-PWA 49.5%	1082	980	896	822

Optical Characterization

The color of BNC/PWA OIN membrane after exposure to UV light changes from colorless to a bluish semi-transparent sheet, as observed in **Figure 1B**. The intensity of the color is proportional to the UV dose, such that longer exposure times more intense is the color. From **Figures 1B**, **2A**, it can be inferred that the distribution of the PWA in the membranes seems to be efficient and a homogeneous blue color is observed after irradiation. The exposed OIN membranes were analyzed by UV-Vis spectroscopy (**Figures 6A,B**). It is important to point out that non-exposed membranes did not present absorption bands in the analyzed

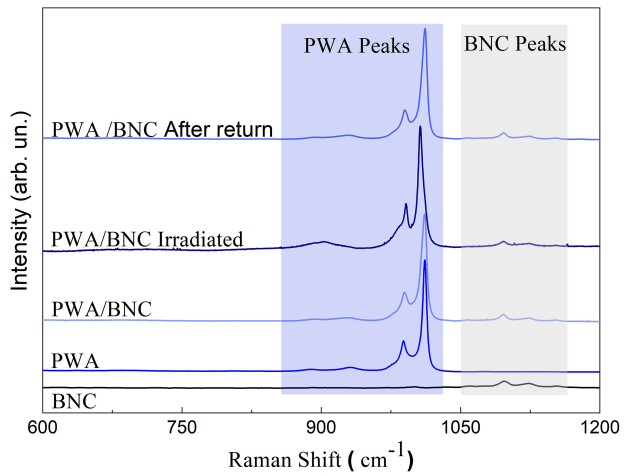

FIGURE 4 | Raman spectra of BNC, PWA, BNC/PWA 49.5% before and after irradiation. The blue and gray regions correspond to PWA and BNC bands, respectively.

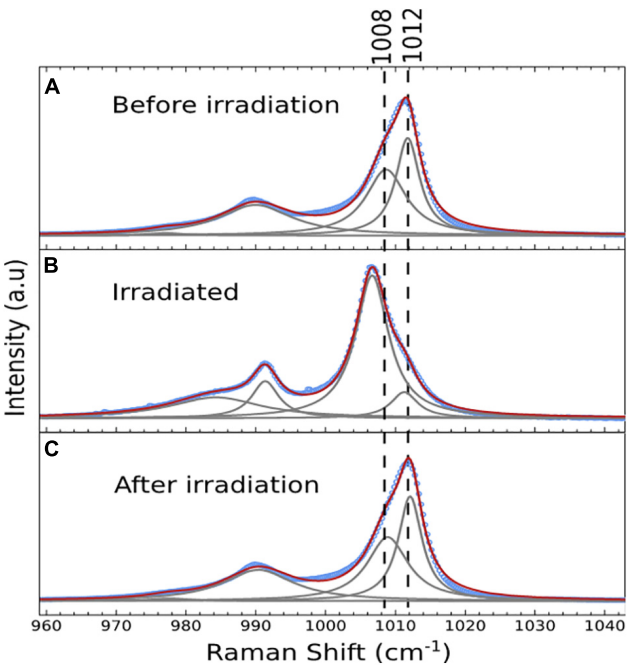

FIGURE 5 | Zoom in the blue region of Raman spectra. The blue dots are the experimental data, the plain gray lines are the four symmetric and asymetric peaks obtained from nonlinear mean square fitting procedure and the plain red line is the sum of the fitted peak adjusting the experimental data. In panel **(A)** the non-irradiated BNC/PWA spectra, **(B)** irritated and **(C)** after irradiation.

spectral range. After exposure, three main absorption bands rose up at 490, 780, and 1,500 nm. The lower energy bands have been assigned to intervalence metal-metal charge transfer (IVCT) involving tungsten sites, according to the equation below.

$$h\nu + W^{5+}(A) + W^{6+}(B) \rightleftarrows W^{5+}(B) + W^{6+}(A)$$

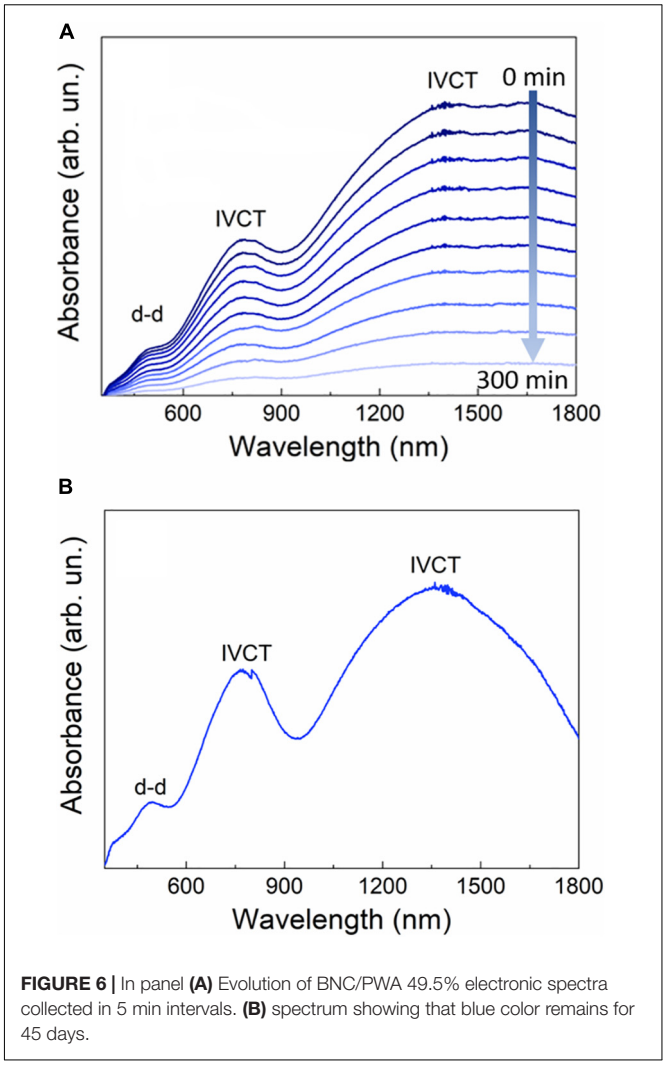

FIGURE 6 | In panel **(A)** Evolution of BNC/PWA 49.5% electronic spectra collected in 5 min intervals. **(B)** spectrum showing that blue color remains for 45 days.

The higher energy band is attributed to d-d transitions of the tungsten ions. It is known that under ultraviolet irradiation fully oxidized tungsten (VI) can be reduced to the tungsten(V) sites, that can be reoxidized by exposing the membranes to air. In fact, the oxygen present in the air is enough to regenerate the fully oxidized species. To verify the reversibility of the membrane, the irradiated sample was put into the spectrophotometer and spectra were collected as a function of time. As observed in **Figure 6A**, the photochromic effect vanishes almost completely after 5 h. This mechanism is real in the presence of oxygen, however, if the membranes are left in nitrogen atmosphere or placed in vacuum the blue color remains longer than 45 days (**Figure 6B**). It is possible to accelerate the regeneration process by increasing the concentration of oxygen in the chamber or by heating up the membranes, in agreement with Yamase (1998).

Photo-Electrochromic Effect

Figure 7A shows cyclic voltammograms of the BNC/PWA 45% OIN from +1.0 to −0.75 V/ (Ag/AgCl/KCl_{sat}) at different scan rates. In 0.2 M Na_2SO_4 aqueous acid solution (pH 2) the hybrid

composite presented three successive and quasi-reversible redox processes, located at $E_{1/2}$ ((E_{pc} +E_{pa})/2) +0.023, −0.251 and −0.693 V/(Ag/AgCl/KCl_{sat}), with the cathodic and anodic peaks separations of 72, 84, and 85 mV, respectively. In general, PWA and other Keggin hetero-polyacids structures exhibit a series of well-resolved one-electron redox processes in neutral or slightly acidic aqueous media, but they merge into two or more electron transfer reactions in strong acid aqueous solution (Sadakane and Steckhan, 1998; Ueda et al., 2017). Also, the two-electron redox activity of PWA are accompanied by protonation and pH has a strong effect on its electrochemical behavior. Thus, the three successive redox couples at +0.023, −0.251 and −0.693 V/(Ag/AgCl/KCl_{sat}) were attributed to the first (I), second (II) and third (III) two-electron reduction of PWA, as summarized below (Li et al., 2002).

$$H_3PW_{12}^{VI}O_{40} + 2e^- + 2H^+ \rightarrow H_5PW_2^{V}W_{10}^{VI}O_{40} \quad (I)$$

$$H_5PW_2^{V}W_{10}^{VI}O_{40} + 2e^- + 2H^+ \rightarrow H_7PW_4^{V}W_8^{VI}O_{40} \quad (II)$$

$$H_7PW_4^{V}W_8^{VI}O_{40} + 2e^- + 2H^+ \rightarrow H_9PW_6^{V}W_6^{VI}O_{40} \quad (III)$$

As shown in **Figure 7A**, by increasing the scan rates, the anodic and cathodic current peaks of these three processes also increase. Curiously, a linear relationship between the current peaks (i_{pa}) with the square root of the scan rates ($v^{1/2}$) was observed (**Figure 7A**-inset) indicating diffusion controlled processes, instead of a direct function of the scan rate expected for immobilized electroactive species. Moreover, the peak to peak separations of the three redox processes are also larger than expected for a two-electron transfer reaction, and much wider than for immobilized redox species in thin films. Thus, these features may be an indicative that electron-hopping processes in the OIN particles are limiting the heterogeneous electron-transfer from the electroactive PWA centers in the BNC membrane to the electrode, rather than a conventional behavior of conductive thin films on electrodes.

Spectroelectrochemical behavior of the OIN BNC/PWA 49.5% were investigated in the visible and NIR spectral regions, and are shown in **Figures 7B–D**. In **Figure 7B** is shown the first cathodic process (I) of the OIN BNC/PWA 49.5% from +0.15 to −0.15 V in 0.2 M Na_2SO_4 acid solution (pH 2). It is worth

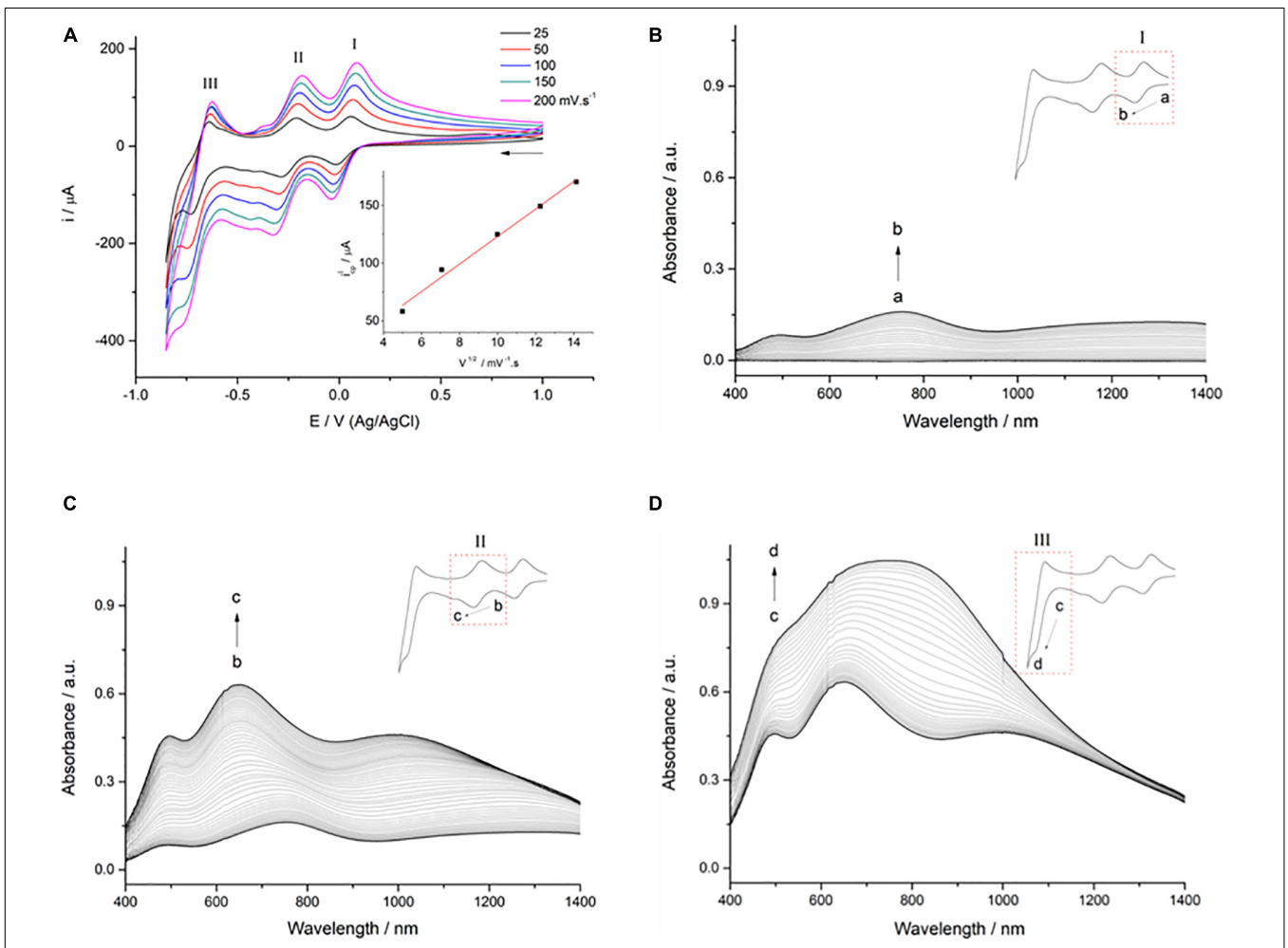

FIGURE 7 | Cyclic voltammograms of the BNC/PWA 49.5% at different scan rates **(A)**. Inset: Linear correlation between the current of the first anodic peak and the square root of scan rates. Spectroelectrochemical behavior of the BNC/PWA 49.5% film associated with the first **(B)**, second **(C)** and third **(D)** cathodic processes.

mentioning that the initial features of OIN BNC/PWA 49.5% membranes immersed in the electrolyte solution are translucent and slightly whitish. As the potential of the first reduction process is achieved, the membrane begins to darken to a bluish hue, and the spectrum is characterized by the rise of three main bands centered at 494, 750, and 1,300 nm. These bands were attributed to a tungsten internal d-d transition and two IVCTs ($W^{5+} \rightarrow W^{6+}$) bands, respectively, as expected for the formation of W^{5+} sites associated to the characteristic two-electron reduction of the Keggin structure (Feng et al., 2002; Cruz et al., 2017).

The spectral shifts associated with the second redox process (II) from −0.15 to −0.45 V are shown in **Figure 7C**. The subsequent reduction of two more tungstate anions ($W^{6+} \rightarrow W^{5+}$) in the polyoxometalate increases the relative number of reduced sites in the Keggin structure, resulting in the increase of the intermetallic IVCTs bands, that shifted from 750 nm and 1,300 nm to 650 and 995 nm. The internal d-d metal band of W^{5+} at 494 nm is shielded and less sensitive to the new electronic configuration of the Keggin polyanion, so only increased in intensity.

Finally, in the last redox process (**Figure 7D**) ranging −0.45 to −0.75 V, the lowest energy IVCT band, that shifts and increases with the third two-electrons reduction of the polyoxotungstate anion, merging with the other IVCT band and resulting in a large convoluted band around 750 nm. Likewise, the internal d-d transition band of W^{5+} at 494 nm only increases with the reduction of other two more tungstate metallic centers. It is worth noting that all processes were still reversible in the timescale of the experiment and similar color changes could be observed in several successive cycles.

CONCLUSION

A simple room temperature route was developed for the fabrication of semi-transparent and free-standing photochromic paper-like nanocomposites based on bacterial nanocelullose (BNC) and phosphotungstic acid (PWA) polyoxometalate. Results obtained by structural and morphological techniques confirm primary Keggin structure is preserved in the nanocomposites, and that BNC network is also stabilizing and controlling PWA nanoparticles in well narrow nanometric size distribution. After exposing BNC/PWA nanocomposite to UV light, there is a change from colorless to a bluish semi-transparent color sheet. The intensity of the blue color is UV dose-dependent and when nanocomposites were exposed to oxygen in air it changed back reversibly. The evaluation of photo-electrochromic effect by spectroelectrochemical measurements reveals reversible photochromic behavior characteristic of the equilibrium between different tungsten oxidation states in the Keggin type material, suggests that all processes were reversible even in several consecutive cycles. Free-standing photochromic BNC/PWA nanocomposites are highly promising to be applied as sensitive displays, reversible data storage, smart windows, among others devices dependent on stimuli-responsive systems.

DATA AVAILABILITY STATEMENT

The original contributions presented in the study are included in the article/supplementary material, further inquiries can be directed to the corresponding author/s.

AUTHOR CONTRIBUTIONS

HB and MS contributed equally to this work and share first authorship. MA, MN, ST, KA, AB, IM, BF, CL, CM, MC, and SR contributed equally to this work. All authors contributed to the article and approved the submitted version.

ACKNOWLEDGMENTS

The authors gratefully acknowledge financial support from FAPESP (#2014/12424-2, #2020/04509-9, #2013/07793-6, #2013/24725-4, and #2016/11591-8). FINEP, CAPES, and CNPq (303137/2016-9). The authors also thank André Tosello Foundation (Campinas-SP, Brazil) for providing the bacterial cellulose strain. HB thanks CNPq (Grant No. 407822/2018-6; INCT-INFO), São Paulo Research Foundation (FAPESP) (Grants No. 2018/25512-8 and No. 2013/07793-6), and TA Instruments Brazil.

REFERENCES

Azeredo, H. M. C., Barud, H., Farinas, C. S., Vasconcellos, V. M., and Claro, A. M. (2019). Bacterial Cellulose as a Raw Material for Food and Food Packaging Applications. *Front. Sustain. Food Syst.* 3:7. doi: 10.3389/fsufs.2019.00007

Barud, H. S., Barrios, C., Regiani, T., Marques, R. F. C., Verelst, M., Dexpert-Ghys, J., et al. (2008). Self-supported silver nanoparticles containing bacterial cellulose membranes. *Mater. Sci. Eng. C.* 28, 515–518. doi: 10.1016/j.msec.2007.05.001

Bretel, G., Le Grognec, E., Jacquemin, D., Hirose, T., Matsuda, K., and Felpin, F.-X. (2019). Fabrication of Robust Spatially Resolved Photochromic Patterns on Cellulose Papers by Covalent Printing for Anticounterfeiting Applications. *ACS Appl. Polym. Mater.* 1, 1240–1250. doi: 10.1021/acsapm.9b00266

Bridgeman, A. J. (2003). Density functional study of the vibrational frequencies of α-Keggin heteropolyanions. *Chem. Phys.* 287, 55–69. doi: 10.1016/S0301-0104(02)00978-3

Casan-Pastor, N., and Gomez-Romero, P. (2005). Polyoxometalates: from Inorganic Chemistry to Materials Science. *ChemInform* 9, 1759–1770. doi: 10.1002/chin.200516227

Chen, J., Liu, Y., Xiong, D. Q., Feng, W., and Cai, W. M. (2008). Preparation and photochromic behavior of crosslinked polymer thin films containing polyoxometalates. *Thin Solid Films*. 516, 2864–2868. doi: 10.1016/j.tsf.2007.05.055

Chen, Z., Yang, Y., Qiu, J., and Yao, J. (2000). Fabrication of Photochromic WO 3 /4,4′-BAMBp Superlattice Films. *Langmuir* 16, 722–725. doi: 10.1021/la9904197

Chiozzini, G. C., Mendes, G. P., Vanni, F. P., Claro, A. M., Amaral, C. S. T., do Amaral, N. C., et al. (2020). Bacterial nanocellulose membrane as bolus in radiotherapy: "proof of concept." *Cellulose* 28, 607–613. doi: 10.1007/s10570-020-03579-8

Cruz, R. P., Nalin, M., Ribeiro, S. J. L., and Molina, C. (2017). Photochromic dynamics of organic–inorganic hybrids supported on transparent and

flexible recycled PET. *Opt. Mater.* 66, 297–301. doi: 10.1016/j.optmat.2017.02.023

Dong, W., Lu, Y., Wang, W., Zhang, M., Jing, Y., and Wang, A. (2020). A sustainable approach to fabricate new 1D and 2D nanomaterials from natural abundant palygorskite clay for antibacterial and adsorption. *Chem. Eng. J.* 382:122984. doi: 10.1016/j.cej.2019.122984

Dufaud, V., and Lefebvre, F. (2010). Inorganic hybrid materials with encapsulated polyoxometalates. *Materials* 3, 682–703. doi: 10.3390/ma3010682

Eichhorn, S. J., Dufresne, A., Aranguren, M., Marcovich, N. E., Capadona, J. R., Rowan, S. J., et al. (2010). Review: current international research into cellulose nanofibres and nanocomposites. *J. Mater. Sci.* 45, 1–33. doi: 10.1007/s10853-009-3874-0

Eichhorn, Y. R. J. (2001). The young's modulus of a microcrystalline cellulose. *Cellulose* 8, 197–207. doi: 10.1023/A:1013181804540

Espindola, A., Gonçalves, N. S., Nalin, M., Ribeiro, S. J. L., Barud, H. S., and Molina, C. (2019). Casting and inkjet printable photochromic films based on polymethylmethacrylate – Phosphotungstic acid. *Opt. Mater.* 96:109345. doi: 10.1016/j.optmat.2019.109345

Feng, W., Zhang, T. R., Liu, Y., Lu, R., Zhao, Y. Y., and Yao, J. N. (2002). Controllable structure and photochromic properties of inorganic-polymeric nanocomposite films. *J. Mater. Sci. Lett.* 21, 497–499. doi: 10.1023/A:1015347026280

Gatenholm, P., and Klemm, D. (2010). Bacterial Nanocellulose as a Renewable Material for Biomedical Applications. *MRS Bull.* 35, 208–213. doi: 10.1557/mrs2010.653

Gutierrez, J., Fernandes, S. C. M., Mondragon, I., and Tercjak, A. (2012). Conductive photoswitchable vanadium oxide nanopaper based on bacterial cellulose. *ChemSusChem* 5, 2323–2327. doi: 10.1002/cssc.201200516

He, T., Ma, Y., Cao, Y., Jiang, P., Zhang, X., Yang, W., et al. (2001). Enhancement effect of gold nanoparticles on the UV-light photochromism of molybdenum trioxide thin films. *Langmuir* 17, 8024–8027. doi: 10.1021/la010671q

He, T., and Yao, J. (2006). Photochromism in composite and hybrid materials based on transition-metal oxides and polyoxometalates. *Prog. Mater. Sci.* 51, 810–879. doi: 10.1016/j.pmatsci.2005.12.001

Hu, W., Liu, S., Chen, S., and Wang, H. (2011). Preparation and properties of photochromic bacterial cellulose nanofibrous membranes. *Cellulose* 18, 655–661. doi: 10.1007/s10570-011-9520-4

Katsoulis, D. E. (1998). A survey of applications of polyoxometalates. *Chem. Rev.* 98, 359–388. doi: 10.1021/cr960398a

Klemm, D., Heublein, B., Fink, H., and Bohn, A. (2005). Cellulose: fascinating Biopolymer and Sustainable Raw Material. *Angew. Chem. Int. Ed.* 44, 3358–3393. doi: 10.1002/anie.200460587

Klemm, D., Kramer, F., Moritz, S., Lindström, T., Ankerfors, M., Gray, D., et al. (2011). Nanocelluloses: a New Family of Nature-Based Materials. *Angew. Chem. Int. Ed.* 50, 5438–5466. doi: 10.1002/anie.201001273

Klemm, D., Schumann, D., Udhardt, U., and Marsch, S. (2001). Bacterial synthesized cellulose - Artificial blood vessels for microsurgery. *Prog. Polym. Sci.* 26, 1561–1603. doi: 10.1016/S0079-6700(01)00021-1

Legnani, C., Barud, H. S., Caiut, J. M. A., Calil, V. L., Maciel, I. O., Quirino, W. G., et al. (2019). Transparent bacterial cellulose nanocomposites used as substrate for organic light-emitting diodes. *J. Mater. Sci. Mater. Electron.* 30, 16718–16723. doi: 10.1007/s10854-019-00979-w

Li, D., Li, W., Sun, C., and Li, A. (2002). Fabrication of carbon paste electrode containing 1:12 phosphomolybdic anions encapsulated in modified mesoporous molecular sieve MCM-41 and its electrochemistry. *Electroanalysis* 14, 368–375.

Qi, W., and Wu, L. (2009). Polyoxometalate/polymer hybrid materials: fabrication and properties. *Polym. Int.* 58, 1217–1225. doi: 10.1002/pi.2654

Rocchiccioli-Deltcheff, C., Thouvenot, R., and Franck, R. (1976). Spectres i.r. et Raman d'hétéropolyanions a-XM12O40n- de structure de type Keggin. *Spectrochim. Acta A* 32, 587–597.

Ross, P., Mayer, R., and Benziman, M. (1991). Cellulose biosynthesis and function in bacteria. *Microbiol. Rev.* 55, 35–58. doi: 10.1128/MMBR.55.1.35-58.1991

Sadakane, M., and Steckhan, E. (1998). Electrochemical properties of polyoxometalates as electrocatalysts. *Chem. Rev.* 98, 219–238. doi: 10.1021/cr960403a

Svensson, A., Nicklasson, E., Harrah, T., Panilaitis, B., Kaplan, D. L., Brittberg, M., et al. (2005). Bacterial cellulose as a potential scaffold for tissue engineering of cartilage. *Biomaterials* 26, 419–431. doi: 10.1016/j.biomaterials.2004.02.049

Tercjak, A., Gutierrez, J., Barud, H. S., Domeneguetti, R. R., and Ribeiro, S. J. L. (2015). Nano- and Macroscale Structural and Mechanical Properties of in Situ Synthesized Bacterial Cellulose/PEO- b -PPO- b -PEO Biocomposites. *ACS Appl. Mater. Interfaces* 7, 4142–4150. doi: 10.1021/am508273x

Torres, F. G., Arroyo, J. J., and Troncoso, O. P. (2019). Bacterial cellulose nanocomposites: an all-nano type of material. *Mater. Sci. Eng. C.* 98, 1277–1293. doi: 10.1016/j.msec.2019.01.064

Ueda, T., Kodani, K., Ota, H., Shiro, M., Guo, S. X., Boas, J. F., et al. (2017). Voltammetric and Spectroscopic Studies of α- And β-[PW12O40]3-Polyoxometalates in Neutral and Acidic Media: structural Characterization as Their [(n-Bu4N)3][PW12O40] Salts. *Inorg. Chem.* 56, 3990–4001. doi: 10.1021/acs.inorgchem.6b03046

Yamase, T. (1998). Photo- and electrochromism of polyoxometalates and related materials. *Chem. Rev.* 98, 307–326. doi: 10.1021/cr9604043

Yang, J., Xiao, Q., Jia, X., Li, Y., Wang, S., and Song, H. (2021). Enhancement of wastewater treatment by underwater superelastic fiber-penetrated lamellar monolith. *J. Hazard. Mater.* 403:124016. doi: 10.1016/j.jhazmat.2020.124016

Conflict of Interest: The authors declare that the research was conducted in the absence of any commercial or financial relationships that could be construed as a potential conflict of interest.